International Association of Geomagnetism and Aeronomy (IAGA)
2nd Symposium: Solar Wind – Space Environment Interaction
December 4th–8th, 2009, Cairo, Egypt – L. Damé & A. Hady (eds)

DOI: 10.1012/S120027852009

Characterization of a CME-driven shock from UV, white light and radio data

Alessandro Bemporad[1] and Salvatore Mancuso[1]

INAF - Turin Astronomical Observatory,
via Osservatorio 20, 10025 Pino Torinese (TO), Italy,
bemporad@oato.inaf.it, mancuso@oato.inaf.it

Abstract. We report on the analysis of a peculiar fast CME–driven shock associated with the eruption of March 22, 2002. The event was observed by the SOHO/UVCS instrument at 4.1 solar radii, with the spectrometer slit placed in correspondence with the flank of the expanding CME. Schock signatures are observed not only in radio dynamic spectra (where a strong type-II radio burst was observed), but also in white light SOHO/LASCO data (as a density gradient located above the expanding CME front) and in SOHO/UVCS spectra (as a strong O VI line broadenings). Interestingly, after the shock transit the observed O VI kinetic temperature slowly decays in ~ 3 hours from $\sim 2\times10^7$ K down to the pre-shock coronal values. This result is in good agreement with the time required for thermalization of O^{5+} ions with protons by collisions. Hence the observed broadening can be attributed mainly to a thermal effect.

Key words: Sun: coronal mass ejections (CME); Sun: UV radiation; Shock waves

1 Introduction

Coronal Mass Ejections (CMEs) are spectacular eruptions of plasma and embedded magnetic fields from the solar surface into the interplanetary space. When a CME occurs, shock waves and solar energetic particles (ions accelerated up to relativistic speeds - SEPs) propagate in the interplanetary medium and possibly impact the Earth magnetosphere producing the most severe space weather events, known as geomagnetic storms. The total mass ejected in CMEs ranges from 10^{13} g to a few 10^{16} g, the total energy (kinetic plus potential energy) from 10^{27} erg to some 10^{33} erg [1], while the CME velocity distribution in the outer corona ranges from ~ 100 km s^{-1} to ~ 2600 km s^{-1}. CMEs propagating faster than the ambient magnetosonic speed eventually drive shocks ahead and may excite type II radio bursts. However, it is at present unclear if a relation of cause-effect between radio bursts and CMEs exists, even because it is generally difficult to differentiate between hot, shock-compressed plasma and coronal ejected plasma.

It has been shown that a few CME-driven shocks are indeed visible also in coronagraphic white light images and that the shock strength can be estimated

[3–5]. Nevertheless, direct imaging of coronal shocks remains an outstanding observational challenge. Moreover, fundamental physical properties of coronal plasma can be derived only through UV spectroscopy, which is able to provide at the same time not only plasma densities, but also coronal plasma temperatures (for electrons and ions), absolute elemental abundances, outflow velocities and crucial information on temperature anisotropies, propagating plasma waves and plasma turbulence. Clear signatures of shock formation in the corona have been reported in the UV spectra [6–10] acquired by the SOHO/UVCS spectrometer [11] as wide and sudden broadenings of spectral line profiles, together with simultaneous brightening of the spectral lines from heavier ions, temporally associated with white light leading edges and type II radio emission.

On 2002 March 22 a fast CME occurred; the event was seen propagating in LASCO/C2 images at the West limb with a projected velocity of $\sim$ 1750 km s^{-1} and was associated with a M-class flare and strong metric and decametric type-II radio emission. The event has also been observed by UVCS, with clear signatures of the shock transit detected in the post-shock UV spectra. In this work, we report on the analysis of the UV spectra associated with the CME-driven shock that have been used to infer properties of the post-shock plasma. After a general description of the event (§ 2), we describe the UVCS data and the analysis we performed (§ 3) and we give our conclusions (§ 4).

2 The March 22, 2002 event

The evolution of the white light corona during the event reported here is shown in Fig. 1. This Figure is a sequence of 3 base difference LASCO/C2 images acquired between 11:06 and 11:54 UT on March 22, 2002. A bright front appears in the 11:06 UT image (left panel) located above the LASCO/C2 occulter with the top at $\sim$ 2.7 $R_\odot$, centered at the latitude of $\sim$ 10°S; the front is surmounted by a weakly brighter hemispherical region located $\sim$ 0.3 $R_\odot$ above the front. In agreement with previous works [3, 4], we identify the white light brightening located above the CME front as a signature of the density compression associated with the transit of the CME-driven shock, propagating faster than the CME. At 11:30 UT (middle panel) the CME front has expanded up to $\sim$ 5.6 $R_\odot$, while the shock front is already out of the LASCO/C2 field of view, hence higher than $\sim$ 6 $R_\odot$. This means that, on average, the CME expanded at $v_{CME} \simeq 1400$ km s^{-1}, while the shock expanded with $v_{sh} > v_{CME}$. At 11:54 UT (right panel) both the CME and the shock fronts exited from the LASCO/C2 field of view. Fig. 1 also shows the position of the UVCS slit field of view; UVCS data are described in the next Section.

The event described above likely originated from the Active Region (AR NOAA 09866) located at the West limb on March 22; this AR is the source of the M-class flare, which occurred with start and peak times of $\sim$ 10:12 and $\sim$ 11:14 UT, respectively. This AR was also the source of a strong continuous radio emission in the 164.0 MHz band, as also observed in previous days by the Nancay Radioheliograph. Interestingly, during the CME release, an enhanced 164.0 MHz

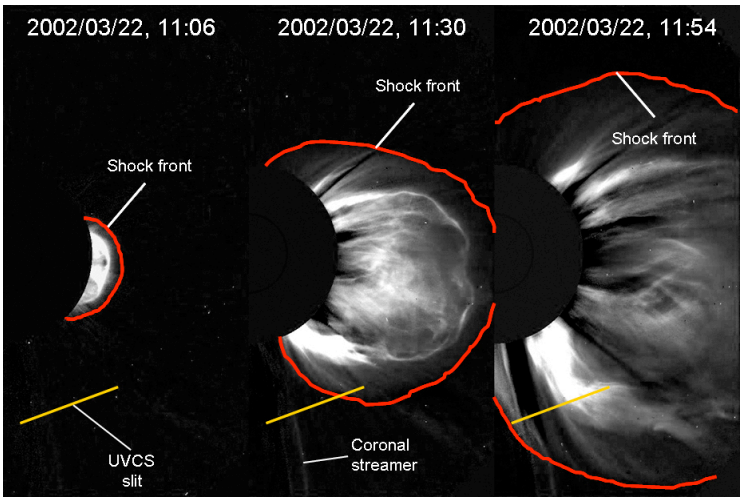

Fig. 1. Sequence of LASCO/C2 base difference images obtained by subtracting from each frame the last one acquired before the CME entrance in the coronagraph field of view; the solid yellow line shows the position of the UVCS slit field of view centered at 4.1 $R_\odot$. Base difference images reveals the existence of a nearly hemispherical density enhancement located above the CME front: we identified this as the compression due to the passage of the CME-driven shock. Hence, this sequence shows the position of the shock front before (left, 11:06 UT), during (middle, 11:30 UT), and after (right, 11:54 UT) its passage through the UVCS slit.

emission appears above the AR. The emitting region is arch-shaped and centered ~ 0.4 $R_\odot$ above the limb at the approximate latitude where the CME erupted; this radio emission is attributable to the front of the CME-driven shock. Later on, a strong type-II radio burst has been detected by the WAVES experiment on the Wind spacecraft. Type-II burst are attributed to shock-accelerated beams of electrons exciting plasma waves that in turn convert into e.m. radiation emitted at the local plasma frequency $f_{pe} \propto \sqrt{n_e}$, where n_e (cm^{-3}) is the local electron density, and/or its harmonic. Hence, the characteristic frequency drift observed during the radio burst is due to the progressive decrease in n_e as the CME-driven shock front expands in the corona.

3 UVCS data description and analysis

The UVCS instrument acquired spectra between 00:55 and 18:29 UT, with an exposure time of 200s, hence yielding a full time coverage during the event. The slit, 40 arcmin long, was centered at the heliocentric distance of 4.1 $R_\odot$ at a latitude of 70°SW; hence the slit was not centered at the central CME latitude and covered a latitude interval between 50.4°S-85.9°S. For this reason, as it is shown in Fig. 1, we expect to observe in the UVCS data a signature of the fraction of the shock front expanding above the southward CME flank. In

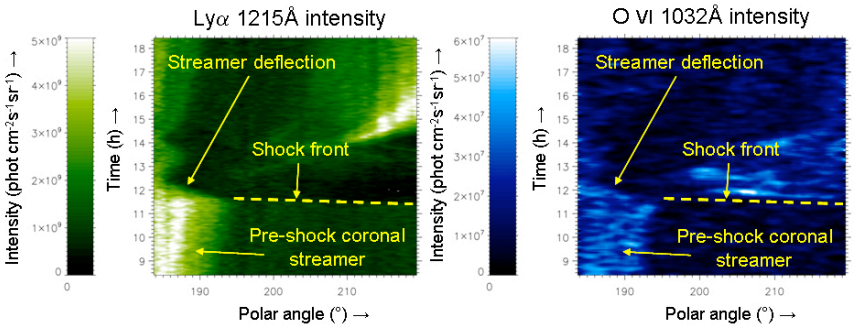

Fig. 2. The evolution with time (y axis) of the H Lyman-α 1215.6 Å (left) and the O VI 1031.9 Å (right) integrated line intensities at different latitudes along the slit (x axis). A clear signature of the shock transit across the slit is observed between 11:20-12:00 UT.

particular, LASCO images show that around 11:30 UT (middle panel) the shock crossed the slit, while approximately 26 minutes later at 11:56 UT the shock was at the southward edge of the slit (right panel).

The observed intensity evolution (Fig. 2) of the two main spectral lines detected during the event confirms the above identification of the shock front from LASCO images. In particular, the H Lyman-α 1215.6 Å line (left) and the O VI 1031.9 Å (right) show an interesting evolution between 11:20-12:00 UT, while other detected spectral lines gave only a weak signal. Differences between the evolution of the two lines shown in Fig. 2 are due to the different physical processes responsible for their emission. In fact, in typical coronal conditions, the H I Lyman-α line is solely due to the radiative excitation (i.e., excitation of atomic levels due to the absorption of photons emitted from the underlying levels of the solar atmosphere), followed by spontaneous emission, while the O VI line is also collisionally excited (i.e., atomic excitation due to collisions with thermal electrons). The main differences are that the radiative component is roughly proportional to n_e and is also dependent on the outflow velocity v_{out} via the Doppler dimming/pumping effect [12], while the collisional component is roughly proportional to n_e^2 and is not dependent on v_{out}. After the transit of the shock front, the Lyman-α dimming due to the plasma acceleration is much larger than the intensity increase due to shock compression and density increase, leading to the observed post-shock intensity decrease (Fig. 2, left panel). At the same time, the radiative component of the O VI line is washed out by the Doppler dimming effect, while the collisional component increases as n_e^2, resulting in the observed post-shock intensity increase (Fig. 2, right panel). Fig. 2 also shows that, as the shock propagates through the slit, a deflection of a southward streamer is observed, as expected when a shock interacts with a streamer structure.

Clear signatures of the shock transit are also visible in the line profile evolution. In the optically thin corona the observed post-shock line profiles are due

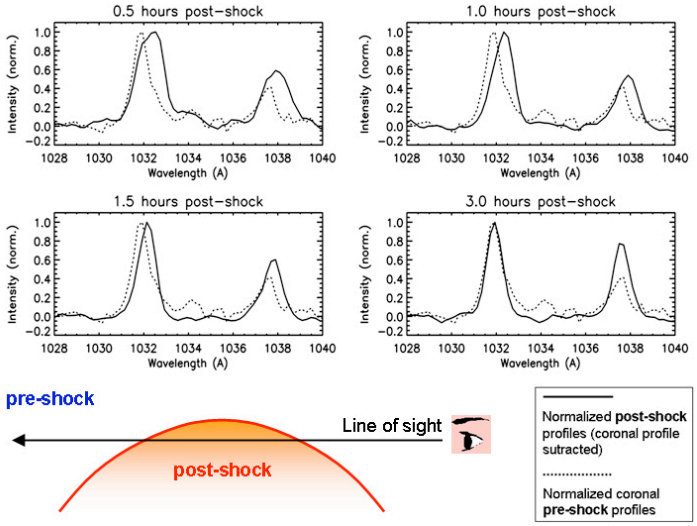

Fig. 3. Top: the evolution as a function of time of the O VI 1037.6-1031.9 Å normalized line profiles for the post-shock plasma (solid line) with respect to the pre-shock coronal profiles (dotted line). About 0.5 hours after the shock transit a strong line broadening and a Doppler shift are observed while, approximately 3 hours later, the pre-shock profiles are recovered. Bottom: a cartoon showing a possible interpretation for the observed evolution. Line broadening is due to both plasma heating and bulk motions of the expanding shock front, while the Doppler shift is likely due to a velocity component of the front in the direction parallel to the line of sight.

to contributions along the line of sight of both the shocked and the unshocked plasmas. Hence, in order to isolate the profiles of the shocked plasma, we removed from the post-shock profiles the average profile observed in the pre-shock corona. Resulting pre- and post-shock profiles of the O VI 1037.6-1031.9 Å lines are shown in Fig. 3 (top), normalized to the peak value of the O VI 1031.9 Å line. Post shock profiles have been averaged over 30 minutes of observations (i.e., 9 exposures) in order to increase the signal to noise ratio. It turns out that, after the shock transit, a strong broadening of both the O VI 1037.6-1031.9 Å is observed, together with a small Doppler shift. In particular, from a Gaussian fitting of the observed profiles, it turns out that the kinetic temperature T_k of the O^{5+} ions increased up to $\simeq 2.0 \times 10^7$ K with respect to a pre-shock kinetic temperature of $\simeq 9.5 \times 10^6$ K. Hence, this result points to a temperature increase by more than a factor of 2. Nevertheless, the observed broadenings are likely due not only to shock heating, but also to bulk motions of the expanding shock front (see Fig. 3, bottom left cartoon). In order to disantangle the two effects, information on the unknow 3-D geometry of the expanding shock front is needed; hence, the kinetic temperature given above has to be considered only as an upper limit to the actual value.

Interestingly, the observed evolution with time of the line profiles shows that $\sim$ 3 hours after the shock transit the pre-shock conditions are mainly recovered. Even though after $\sim$ 3 hours the O VI 1037.6-1031.9 Å FWHMs and centroid positions of shocked plasma are, within the uncertainties, equal to the values observed in the pre-shocked corona, the ratio between the O VI 1037.6-1031.9 Å lines is changed. In particular, after the shock, the ratio between the intensities of the O VI 1031.9 Å and the O VI 1037.6 Å lines is much smaller than what observed in the pre-shock corona (see Fig. 3, bottom right panel). Because this ratio is dependent on the plasma outflow velocity [12], this evolution suggests that $\sim$ 3 hours after the shock transit any kinetic temperature increase of the O^{5+} ions has been thermalized back to the pre-shock coronal values, while the larger outflow velocity of post-shock accelerated plasma is preserved. Thanks to the long duration of spectroscopic observations reported here, this is the first time that it has been possible with UVCS to study the evolution of post-shock coronal plasma.

4 Conclusions

On 2002 March 22 a fast ($\sim$ 1400 km s^{-1}) CME was observed simultaneously by the LASCO/C2 coronagraph and the UVCS spectrometer. The event was associated with strong radio emission observed both as a metric (164 MHz) arch shaped emission located above the source Active Region and also as a type-II decametric emission with typical frequency drift from $\sim$ 10 down to $\sim$ 1 MHz. These radio observations are in agreement with the presence of a CME-driven shock expanding through the corona above the CME front. A clear signature of the shock front was also observed in LASCO/C2 white light images as a weak hemispherical density gradient located above the expanding CME front. The shock has also been observed by the UVCS instrument, whose slit was located at the heliocentric distance of 4.1 $R_\odot$ in correspondence with the CME southward flank. The shock transit is shown by a clear signature not only in the H I Lyman-α 1215.6 Å and O VI 1031.9 Å line intensity evolutions, but also in the evolution of respective line profiles. In particular, strong line broadenings are detected, indicative of a kinetic temperature increase of O^{5+} ions by approximately a factor of 2 with respect to the pre-shock corona. Interestingly, $\sim$ 3 hours after the shock transit the pre-shock kinetic temperatures are mainly recovered. This long time interval required to recover the pre-shock kinetic temperature suggests that the broadening reported here is mainly a thermal effect, because we expect a much faster decay for the broadening due to the bulk expansion of a shock moving at more than 1000 km s^{-1}. In particular, by assuming for a high latitude coronal region at 4.1 $R_\odot$ a proton density $n_p = 10^5$ cm^{-3} and a proton temperature $T_p = 2 \times 10^6$ K [13], it turns out that the time τ_{eq} required for the equipartition of energy between protons and O^{5+} ions with a kinetic temperature of $T_k = 2.0 \times 10^7$ K is $\tau_{eq} \simeq 2.7$ hours. This time is in good agreement with the observed $\sim$ 3 hours of T_k decay, due to the thermalization with protons of O^{5+} ions heated by the shock transit. Moreover, $\sim$ 3 hours after the shock transit the

ratio between the intensities of the O VI 1031.9 Å and the O VI 1037.6 Å lines is much smaller than what observed in the pre-shock corona. This lower ratio indicates that significative plasma outflows are present in the post-shock corona, even hours after the shock transit. Hence, this result seems to indicate that at the CME flank the coronal magnetic field, left open by the CME transit, has not yet recovered the pre-CME configuration and that this angular sector of the corona has been converted by the CME transit in a fast wind region. This is the first time that the evolution of post-shock coronal plasma has been studied with UVCS data.

Acknowledgments. A.B. acknowledges support from ASI/INAF I/023/09/0 contract and from the Italian Embassy within the Egypt-Italy Science Year (EISY) 2009 Program. SOHO is a project of international cooperation between ESA and NASA.

References

1. Gopalswamy, N., et al.: Variability of solar eruptions during cycle 23. Adv. in Space Res., 34, 391–396 (2004)
2. Yeh, C.-T., et al.: Waiting Time Distribution of Coronal Mass Ejections. Chinese J. of Astron. & Astroph., 5, 193–197 (2005)
3. Vourlidas, A., et al.: Direct Detection of a Coronal Mass Ejection-Associated Shock in Large Angle and Spectrometric Coronagraph Experiment White-Light Images. Astrophys. J., 598, 1392–1402 (2003)
4. Ontiveros, V., & Vourlidas, A.: Quantitative Measurements of Coronal Mass Ejection-Driven Shocks from LASCO Observations. Astrophys. J., 693, 267-275, (2009)
5. Mancuso, S., & Bemporad, A.: Interpretation of the SOHO/UVCS observations of two CME-driven shocks. Adv. in Space Res., 44, 451-456 (2009)
6. Raymond, J.C., et al.: SOHO and radio observations of a CME shock wave. Geophys. Res. Lett. 27, 1439-1442 (2000)
7. Mancuso, S., et al.: UVCS/SOHO observations of a CME-driven shock: Consequences on ion heating mechanisms behind a coronal shock. Astron. & Astrophys. 383, 267-274, (2002)
8. Raouafi, N.-E., et al.: Shock wave driven by an expanding system of loops. Astron. & Astrophys., 424, 1039–1048 (2004)
9. Ciaravella, A., et al.: Detection and Diagnostics of a Coronal Shock Wave Driven by a Partial-Halo Coronal Mass Ejection on 2000 June 28. Astrophys. J., 621, 1121–1128 (2005)
10. Mancuso, S., & Avetta, D.: UV and Radio Observations of the Coronal Shock Associated with the 2002 July 23 Coronal Mass Ejection Event. Astrophys. J., 677, 683-691 (2008)
11. Kohl, J.L., et al.: The Ultraviolet Coronagraph Spectrometer for the Solar and Heliospheric Observatory. Sol. Phys., 162, 313-356 (1995)
12. Noci, G., et al.: Solar wind diagnostics from Doppler-enhanced scattering. Astrophys. J., 315, 706–715 (1987)
13. Antonucci, E., et al.: Slow wind and magnetic topology in the solar minimum corona in 1996-1997. Astron. & Astrophys., 435, 699–711 (2005)